GA–A23967

EXPLICIT CALCULATIONS OF HOMOCLINIC TANGLES SURROUNDING MAGNETIC ISLANDS IN TOKAMAKS

by
R.K.W ROEDER, B.I. RAPOPORT, and T.E. EVANS

JUNE 2002

DISCLAIMER

GA–A23967

EXPLICIT CALCULATIONS OF HOMOCLINIC TANGLES SURROUNDING MAGNETIC ISLANDS IN TOKAMAKS

by
R.K.W ROEDER,* B.I. RAPOPORT,† and T.E. EVANS

This is a preprint of a paper to be submitted for publication in *Phys. Plasmas.*

*Department of Mathematics, Cornell University, Ithaca, New York.
†Harvard University, Cambridge, Massachusetts.

Work supported by
the U.S. Department of Energy under
Contract No. DE-AC03-99ER54463

GENERAL ATOMICS PROJECT 30033
JUNE 2002

ABSTRACT

We present explicit calculations of the complicated geometric objects known as homoclinic tangles that surround magnetic islands in the Poincaré mapping of a tokamak's magnetic field. These tangles are shown to exist generically in the magnetic field of all toroidal confinement systems. The geometry of these tangles provides an explanation for the stochasticity known to occur near the X-points of the Poincaré mapping. Furthermore, the intersection of homoclinic tangles from different resonances provides an explicit mechanism for the non-diffusive transport of magnetic field lines between these resonance layers.

I. INTRODUCTION

In this paper we provide an explicit calculation of the complicated geometric objects known as homoclinic tangles in the Poincaré mapping of a tokamak's magnetic field. Although homoclinic tangles are known to be a generic property of conservative Hamiltonian systems [1–3], the detailed structure of these tangles has not previously been studied for realistic tokamak geometries. Such calculations are valuable, since homoclinic tangles are expected to be a property of all toroidal confinement systems such as tokamaks, stellarators, and RFP's. Our calculations illustrate the genericness of homoclinic tangles surrounding the magnetic island chains in toroidal confinement devices. These tangles contribute heavily to the stochasticity that is known to occur in the magnetic field of a tokamak. Moreover, they provide an explicit mechanism for the non-diffusive transport of magnetic field lines across adjacent resonant layers when the tangles surrounding neighboring islands intersect. (This paper is a more detailed exposition on the ideas that were presented as a poster in [4].) We begin by reviewing some of the standard background necessary for understanding this geometry.

It is a well known fact that the vacuum magnetic field in a tokamak can be expressed as a time dependent one degree of freedom Hamiltonian system [5–7]. The system is expressed as:

$$\frac{d\theta}{d\phi} = \frac{\partial H(\theta,\psi,\phi)}{\partial \psi} \quad , \qquad \frac{d\psi}{d\phi} = -\frac{\partial H(\theta,\psi,\phi)}{\partial \theta} \quad , \tag{1.1}$$

where ϕ is the toroidal variable (canonical time), θ is the poloidal variable (canonical coordinate), and ψ is the momentum conjugate to θ. One can think of ψ as a radius-like variable. The dependence of H on ϕ is a result of resonant helical magnetic perturbations imposed either intentionally or unintentionally in the flux surface equilibria of toroidal confinement systems. Tokamaks, for example, are designed to be toroidally symmetric but, in reality, they are known to suffer from error fields due to initial construction irregularities and changes in the magnetic components due to unbalanced electromagnetic forces and thermal stresses during both standard operations and off-normal events.

However, since a tokamak is designed to have toroidal symmetry, the Hamiltonian H is a small perturbation from an integrable one. Hence, our system fits within the context of the abundant literature on near-integrable systems, including [8] and [9].

Throughout this paper we will focus on the dynamics of a Poincaré mapping P of a surface Γ of constant ϕ. For $x \in \Gamma$, $P(x)$ is determined by the point where the unique field line through x intersects Γ after one (counterclockwise) toroidal transit. Standard results from the theory of ordinary differential equations imply that P is a *diffeomorphism*, that is, a differentiable mapping with differentiable inverse. In addition, for Hamiltonian systems of the form (1.1) P is known to be area preserving.

There are certain common features of the phase portraits resulting from Poincaré mappings of near-integrable systems of the form (1.1). In particular, there are the well known KAM surfaces which appear as invariant simple closed curves [1,10]. Between these KAM

surfaces are the resonant tori corresponding to the tori from the integrable system which had rational rotation numbers and have been destroyed by resonance [1,10]. On a coarse level, the geometry of these resonant tori consists of a series of small closed invariant curves known as *islands* surrounding elliptic periodic points known as *O-points*. Between these islands are hyperbolic periodic points known as *X-points*.

We are interested in the finer geometry surrounding these islands described by the invariant associated with the X-points. The stable manifold $W^s(x_0)$ of a (hyperbolic) fixed point x_0 consists of the set of points in the Poincaré section that converge to x_0 under forward iteration of the map and the unstable manifold $W^u(x_0)$ consists of the set of points that converge to x_0 under backwards iteration of the map:

$$W^s(x_0) = \{x \mid P^{(n)}(x) \to x_0 \; as \; n \to \infty\} \quad , \tag{1.2}$$

$$W^u(x_0) = \{x \mid P^{(n)}(x) \to x_0 \; as \; n \to -\infty\} \quad . \tag{1.3}$$

Given a point of period m, one merely considers it as a fixed point of $P^{(m)}$ and applies the definition above, replacing P with $P^{(m)}$. These sets of points are called "manifolds" since they have been proven to be continuous curves with no self-intersections and are called invariant since $P[W^s(x_0)] = W^s(x_0)$ and $P[W^u(x_0)] = W^u(x_0)$. They are also known to approach tangentially the eigen-directions of the linearization of P at x_0. The reader is encouraged to consider the following sources for more information on invariant manifolds [3,10,11]. See Fig. 1 for an illustration of finite portions of the invariant manifolds of an X-point. The reader may wish briefly to skip to Section III to see some numerically calculated invariant manifolds (the real thing) before continuing.

These manifolds have a physical interpretation, in the context of the Poincaré mapping from a tokamak: since $P(x)$ is defined as the point where the unique field line through x intersects Γ after one counter-clockwise toroidal transit, the (un)stable manifold of a period one X-point is given by the set of all points on Γ which lie on field lines that converge to the X-point under infinitely many (clockwise) counter-clockwise toroidal transits. The reader may wish to consider how this interpretation generalizes to X-points of higher periods.

When these manifolds surround the "islands" there are two possibilities: the stable (respectively unstable) manifold from a certain x-point can cross the unstable (respectively stable) manifold from the next X-point in the island chain either transversely or tangentially. In the case where they meet tangentially, one has a single invariant curve connecting the two fixed points, known as a separatrix. However, for a generic system they cross transversely [1–3].

For this reason, the case of a transverse intersection point x is of particular interest. The forward and backward iterates of x are also intersections because both manifolds are invariant under P, and these intersections are transverse because P is a diffeomorphism. Mapping x under $P^{(n)}$ for each integer n we find that there are infinitely many transverse intersections which approach the X-points as $n \to \pm\infty$ since these points of intersection are on the stable manifold of one of the fixed points and the unstable manifold of the other. The region enclosed within the two invariant manifolds between two subsequent intersection points is

referred to as a *lobe* (Fig. 2). One can check that *P* maps one lobe to the next lobe (of the same orientation), causing the area of each lobe to be the same because *P* is area preserving. This presents a dilemma since the width of the bases of the lobes becomes arbitrarily small near the X-points. To compensate for this, these lobes must become arbitrarily long and skinny. This leads to quite a complicated geometry since the invariant manifolds must then wind in increasingly more complicated ways to avoid self-intersection while the lobes get arbitrarily long and skinny near the X-points. Such geometric objects are known as *homoclinic tangles* [1,10,12,13]. See Fig. 2 for a depiction of a separatrix and a finite portion of a homoclinic tangle. For an excellent exposition of much of what we have presented above, please see [3].

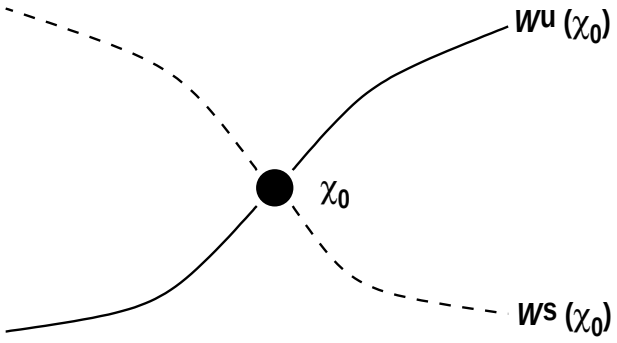

Fig. 1. Invariant manifolds of an X-point.

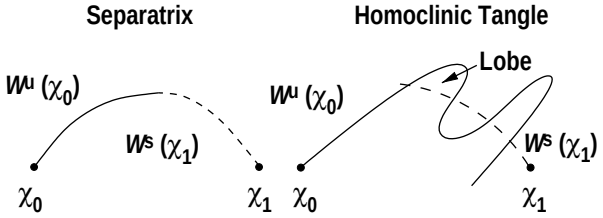

Fig. 2. Separatrix and homoclinic tangle.

II. MODELS FOR THE MAGNETIC FIELD IN A TOKAMAK

We consider both the Tokamap [14] and Tripmap (based on the TRIPND field line integration code [15]) models for the magnetic field in a tokamak. The Tokamap model provides a closed form expression which is designed to satisfy the basic requirements of the Poincaré mapping resulting from a tokamak's magnetic field. Specifically, the Tokamap conforms with the constraints of the toroidal geometry of a tokamak and satisfies a twist (safely factor) profile that is realistic for a tokamak. The tokamap is given by:

$$\psi_{n+1} = \psi_n - \frac{K}{2\pi}\frac{\psi_{n+1}}{(1+\psi_{n+1})}sin(2\pi\theta_n) \quad , \tag{2.1}$$

$$\theta_{n+1} = \theta_n + W(\psi_{n+1}) - \frac{K}{(2\pi)^2}\frac{1}{(1+\psi_{n+1})^2}cos(2\pi\theta_n) \quad , \tag{2.2}$$

$$W(\psi_{n+1}) = \frac{w}{4}(2-\psi_{n+1})(2-2\psi_{n+1}+\psi_{n+1}^2) \quad , \tag{2.3}$$

where θ is the poloidal angle and ψ is the momentum conjugate to θ. The parameter K determines the strength of the perturbation and w controls the slope of the twist profile. To evaluate the mapping, it is necessary to use the quadratic formula to solve (2.1) for ψ_{n+1}, choosing the positive root. While it would be hard to obtain an expression for the inverse of the tokamap, one can numerically solve Eqs (2.1) and (2.2) for θ_n and ψ_n in terms of θ_{n+1} and ψ_{n+1}.

The other model that we consider is the Tripmap model [15], which has been used to simulate the magnetic field in the TFTR and Tore Supra tokamaks. Instead of trying to write down an expression for a Poincaré mapping, in reference [15] Evans models the actual geometric imperfections in a tokamak. Specifically, eighteen toroidal field coils are placed in a toroidally symmetric configuration, then perturbed by a small random perturbation, introducing the type of asymmetry mentioned in Section I. The magnetic effects of the plasma current are modeled by a current through a single toroidal filament placed on the toroidal axis. Based on the positions of these coils, the magnetic field may be calculated anywhere inside of this hypothetical tokamak. To calculate numerically the Poincaré mapping of the surface $\phi = 0$, any initial condition $(r, \theta, \phi = 0)$ is numerically integrated forward once toroidally around the tokamak. The inverse mapping is easily obtained by integrating once backwards around the tokamak.

III. NUMERICAL DEMONSTRATION OF THE EXISTENCE OF HOMOCLINIC TANGLES

In Fig. 3 we present a numerically calculated phase portrait from the Tokamap and a finite portion of a homoclinic tangle surrounding the (2,1) resonant island. In Fig. 4 we present a numerically calculated phase portrait from the Tripmap and finite portions of the homoclinic tangles surrounding the (1,1), (2,1), and (3,1) resonant islands. We display these homoclinic tangles at quite a large perturbation level so that they are very pronounced; however, they also exist at smaller, more realistic, perturbation levels, as depicted in Fig. 5.

The reader may notice that a homoclinic tangle at a low level of perturbation, as in Fig. 5, appears much like a separatrix. This is the reason why the separatrix approximation method of Chirikov [8] works in low level approximations. However, there are fundamental differences at a finer scale. In particular, the separatrix cannot properly account for the well known stochasticity in a neighborhood of an X-point [16] while homoclinic tangles can. Furthermore, the overlap of separatrices from neighboring resonant islands cannot provide a logically consistent explanation for the mixing of field lines between resonances, while the homoclinic tangle can. We explain these facts in Sections IV and V.

The method used to calculate these portions of the stable and unstable manifolds is quite simple: A minimization routine was used to find the desired X-point. Once the X-point was found, a small interval pointing away from the X-point in the general direction of the unstable (stable) eigenvector was mapped forward (backwards) repeatedly under $P^{(n)}$ (where n is the period of the point x_0) to obtain an approximation of the unstable (stable) invariant manifold. Certainly better algorithms are available and recently the Tripmap was interfaced with the program Dynamics [17] which includes a modern algorithm for calculating the invariant manifolds of a periodic point.

Some may find it surprising that homoclinic tangles exist in the magnetic field of a tokamak. A common cause for this confusion comes from a misunderstanding of the Chirikov overlap criterion [8]. In this calculation, one discards high order terms from the expansion of the Hamiltonian, so that the solution has perfect separatrices with which to estimate the width of the resonant islands. However, for most systems these separatrices are just an idealization. Furthermore, one can actually obtain a more accurate estimate of the perturbation level required for transport between two resonances by computing the homoclinic tangles surrounding islands from neighboring resonances at a few different perturbation levels and determining at what level of perturbation they intersect. (See Section V.)

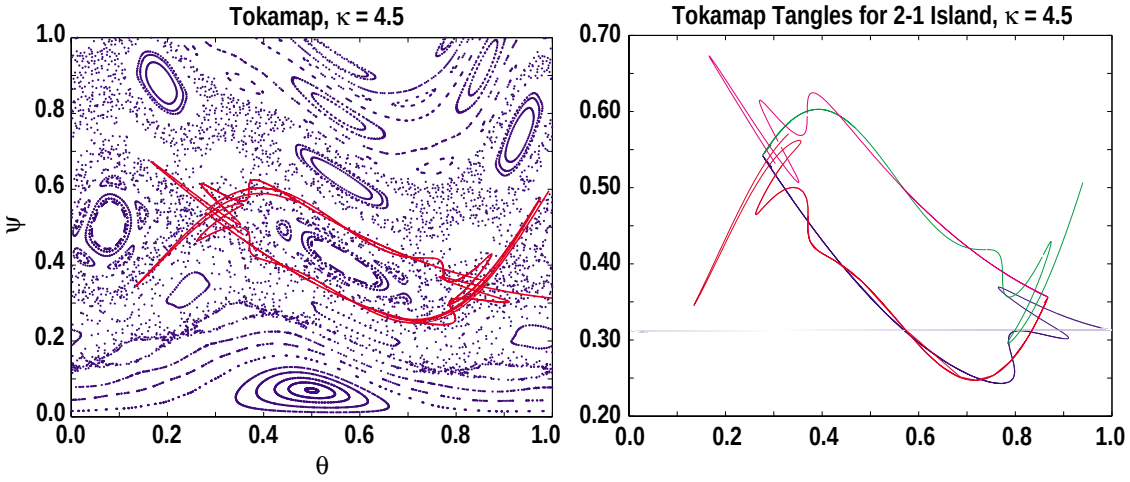

Fig. 3. Phase portrait and the (2,1) homoclinic tangle for the Tokamap.

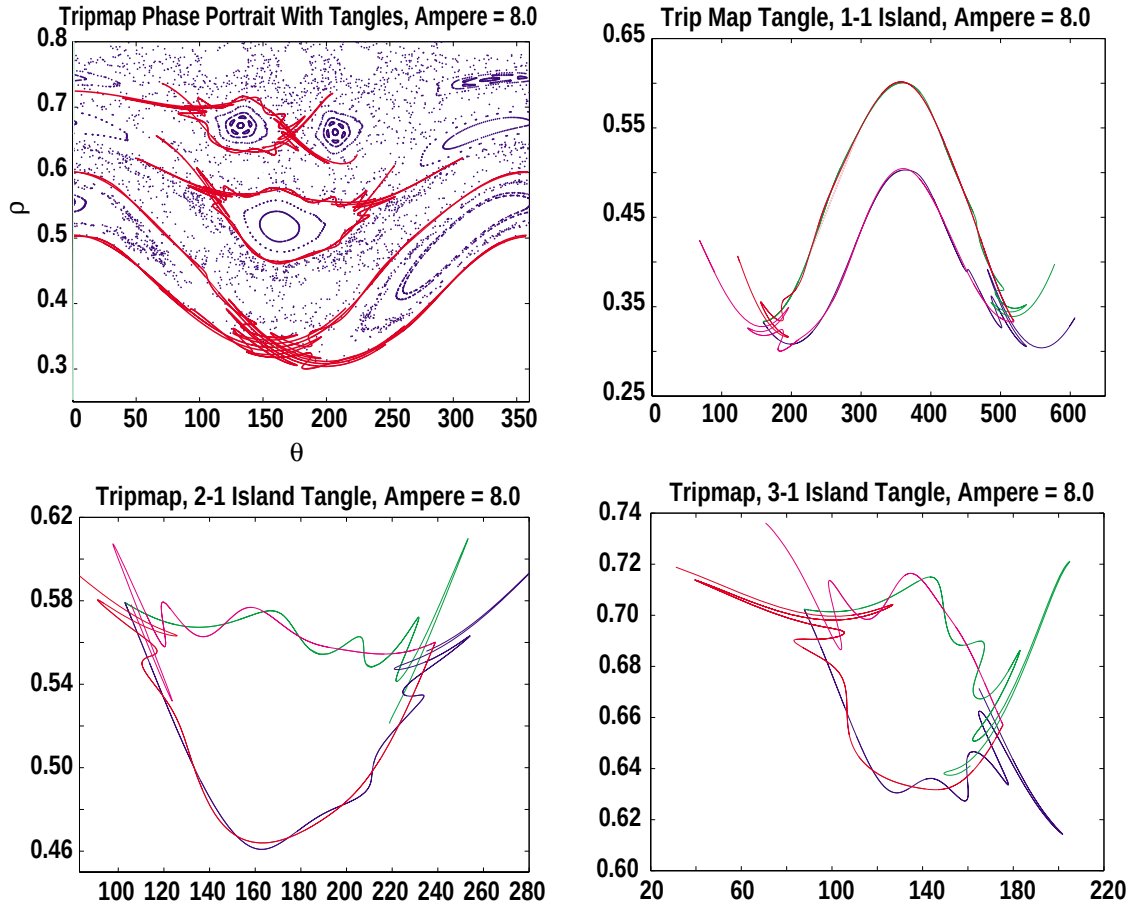

Fig. 4. Phase portrait and the (1,1), (2,1), and (3,1) homoclinic tangles for the Tripmap at a high level of perturbation.

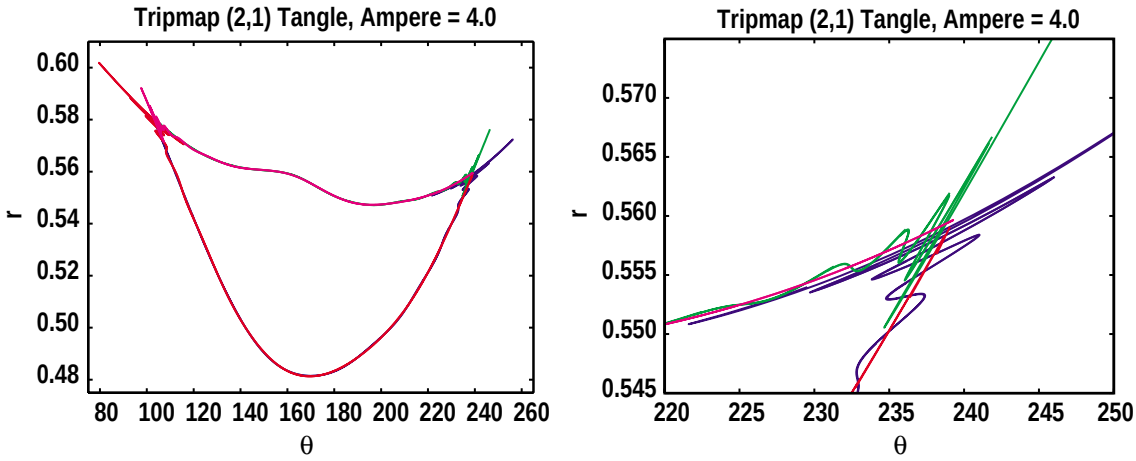

Fig. 5. Tripmap tangle surrounding the (2,1) island and detail of the structure near an X-point at half of the perturbation level of those in Fig. 4.

IV. THE SMALE-BIRKHOFF HOMOCLINIC THEOREM

Although the geometry of a homoclinic tangle is quite complicated, two beautiful theorems characterize much of this complexity in a very clear way:

Theorem 1 (Smale-Birkhoff) *Given a Poincaré mapping $f : \mathbb{R}^2 \to \mathbb{R}^2$ having a homoclinic tangle, then there is a region U in $\mathbb{R}^2$ and some k such that on U the iterate $f^{(k)}$ is topologically equivalent to the Smale horseshoe map F.*

The reader should recall that the Smale horseshoe mapping is the mapping depicted in Fig. 6 and discussed at length in [11]. Also in Fig. 6 is a diagram illustrating how the Smale horseshoe occurs in a homoclinic tangle. For a mathematically precise statement of the Smale-Birkhoff theorem, see [11].

The following theorem outlines the complexity of the dynamics given by the Smale horseshoe mapping, and hence the complexity of the dynamics in a neighborhood of a homoclinic tangle.

Theorem 2 *The Horseshoe map F has an invariant (cantor) set Λ such that:*

1. *Λ contains (countably) infinitely many periodic orbits of arbitrarily long periods,*
2. *Λ contains (uncountably) infinitely many bounded non-periodic orbits, and*
3. *Λ contains a dense orbit.*

Again, for more details, see [11].

In short, these two theorems assert that there is *Hamiltonian chaos* in the magnetic field of a resonantly perturbed tokamak because the tokamak field contains homoclinic tangles. In particular, associated with *each* homoclinic tangle are infinitely many closed field lines of arbitrarily high toroidal winding numbers, and infinitely many chaotic field lines.

A slightly deeper understanding of the Smale-Birkhoff theorem shows that the region where this chaos occurs is always in a neighborhood of the X-points. In this way we see that the Smale horseshoes associated with a homoclinic tangle provide a mechanism for the stochasticity that is known to occur in the neighborhood of the X-points [16]. The notion of a separatrix cannot explain this stochasticity, since the dynamics on a separatrix are elementary.

The chaos associated with homoclinic tangles becomes especially impressive, since homoclinic tangles are expected to exist surrounding each resonant island [1–3], and in general there are infinitely many resonant islands. (In fact the level of complexity is even higher if one considers that there will be homoclinic tangles associated with the higher order resonant structures [1,3].)

One common misconception is that since the magnetic field is divergence free, this type of complicated behavior cannot exist. However, since (1.1) is a Hamiltonian system, the divergence of the vector field is always zero.

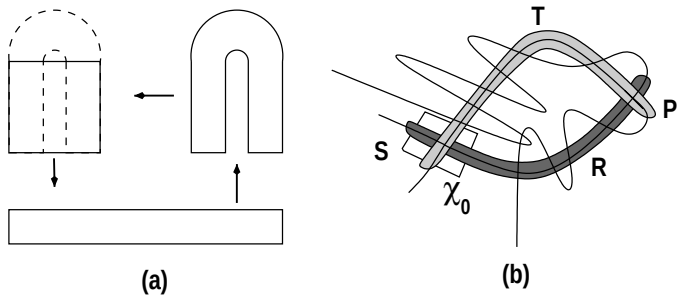

Fig. 6. (a) The Smale horseshoe mapping: The original rectangle (top left) is stretched in an area preserving way, forming an elongated rectangle (bottom). The new rectangle is bent to form a horseshoe (top right) and superimposed on the original rectangle (dashed horseshoe, top left). A point in the original rectangle is mapped to the point on which it lands, inside the original rectangle, after undergoing the deformations just described. Notice that a region is lost after each iteration. (b) An illustration of *where* a Smale horseshoe is found in a homoclinic tangle. A region S surrounding x_0 forms the narrow region R covering a segment of the stable manifold when mapped under $P^{(-m)}$. Similarly, region S forms the narrow region T covering a segment of the unstable manifold when mapped under $P^{(n)}$. Regions R and Tmust intersect at the fixed point x_0. However, m and n can be chosen so that regions R and T contain the homoclinic point p, causing them to intersect at p, as well. In this case, they form a topological version of the Smale horseshoe with $P^{(m+n)}$ mapping R to T, as depicted above. The regions R and T in (b) correspond, respectively, to the original and horseshoe-mapped rectangles in the upper left part of (a).

V. TRANSPORT

Since homoclinic tangles are expected to surround each resonant island, it is natural to ask whether there is any interaction between homoclinic tangles from different resonant tori. In fact, they can intersect, as depicted in Fig. 7.

Intersecting homoclinic tangles provide a clear mechanism for the anomalous transport of particles along field lines from one resonance layer to the next. If the lobes from neighboring homoclinic tangles intersect, the region of intersection must undergo the dynamics associated with each individual tangle, hence must "mix" throughout each of the tangles. Figure 8 illustrates the transport of a particle from one tangle to the next.

Understanding figure 8 is crucial to understanding transport between resonant layers. First, notice that the tangles depicted in this figure are assumed to correspond to periodic points of the same period, which we can assume to be of period one. In each tangle, the Poincaré mapping sends a lobe on the bottom part of the tangle to the next one to the right, that has the same orientation, and a lobe on the top part of the tangle to the next one to the left, that has the same orientation. Notice that as the iterates of a lobe cross the midpoint of the tangle, the lobe switches from facing inward towards the center of the tangle to pointing outward, or vice-versa. This enables points that were "inside" of the tangle to get "outside" of the tangle when mapped enough times under the Poincaré mapping.

In the lower tangle of figure 8, consider the point in the lobe that is furthest to the right and "inside" of the tangle. We will see how the field line associated with this point of the Poincaré section can migrate from the lower tangle to the upper tangle. We can determine much of the dynamics of this point by just knowing the dynamics of the lobe containing it. Under P, this point is mapped, with it's lobe, to the left across the top of the bottom tangle. After four iterates of P the point is in the intersection of lobes from the lower and upper tangles. From this point on, we can determine the further iterates of the point using our knowledge of the dynamics of the lobes in the upper tangle. Further iterations of P carry the point to the right, from lobe to lobe, across the bottom of the upper tangle. Eventually, it reaches the far side of the upper tangle at which point it is "inside" of the upper tangle. Hence the field line starting "inside" the lower tangle has made the transition to the "inside" of the upper tangle, *due to an intersection between the two tangles.* The case of tangles corresponding to periodic points of different periods is more common, as in figure 7, but is more difficult and will not be explained in detail in this paper.

There are two advantages to understanding transport between resonances in terms of the intersection of homoclinic tangles. First, they provide a logically consistent explanation of this transport, while the overlap of separatrices cannot. In fact, distinct separatrices cannot overlap, since the points of overlap would be on the stable manifolds from two different X-points, hence would have to converge to two distinct points under forward iteration. The homoclinic tangle overcomes this difficulty since it is split into *distinct* stable and unstable manifolds, allowing the stable manifold from one tangle to cross the unstable manifold from the other.

Second, the intersection of homoclinic tangles can provide a more accurate determination of the level of perturbation necessary for resonant transport. Specifically, as we saw above, if homoclinic tangles from neighboring resonances intersect, there *must* be transport between these resonances. One could calculate homoclinic tangles from a pair of neighboring resonances for a sequence of increasing perturbation levels and approximate the smallest level of perturbation for which the homoclinic tangles intersect. Such a calculation could easily offer a lower, and hence more accurate, prediction than given by the Chirikov criterion [8]. This type of prediction would agree with repeated observations that the Chirikov criterion consistently overestimates the level of perturbation necessary for resonance overlap [1,7].

The reader should notice two difficulties with the above approach: First, if one wanted to show that two homoclinic tangles did not intersect, one would have to compute an infinite length of the invariant manifolds, which is impossible. Second, transport between two resonant layers could happen at lower levels than predicted by either of these approximation methods if there is another resonance layer between the two being considered.

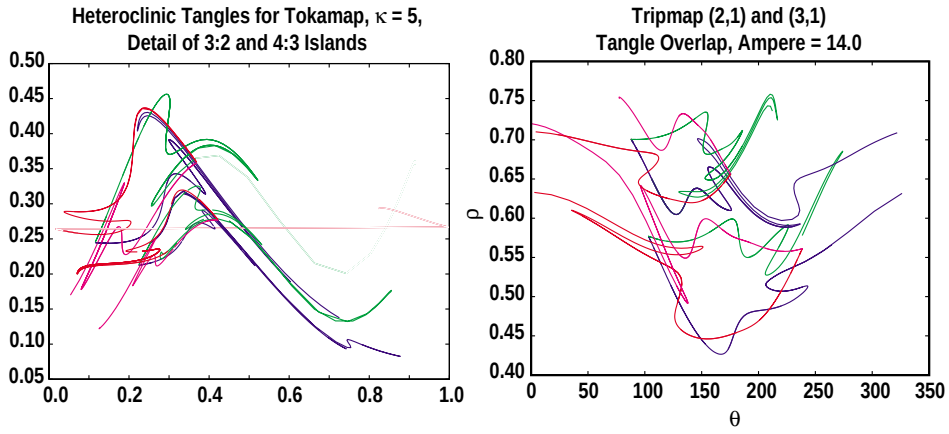

Fig. 7. Homoclinic tangles from neighboring resonances overlap for the Tokamap (left) and for the Tripmap (right).

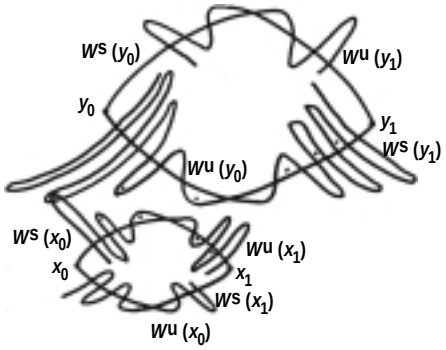

Fig. 8. Intersecting homoclinic tangles lead to transport between resonant layers. The black dots indicate the trajectory of a point making the transition from the lower tangle to the upper tangle.

VI. CONCLUSION

Although homoclinic tangles are known to exist in a generic Poincaré mapping [1–3], we have presented explicit calculations of them for two models of the Poincaré mapping from a tokamak to highlight their relevance in plasma physics. We have also presented two standard theorems that describe some of the geometric complexity in a tokamak's magnetic field which results from the existence of homoclinic tangles. While the generic nature of homoclinic tangle interactions makes them of general interest for understanding mass and energy transport in a range of physical systems, the specific details of these structures in toroidal magnetic confinement systems has a direct impact on the plasma performance and fusion yield.

For collisionless plasmas we consider the intersection of homoclinic tangles from neighboring resonant tori to be a prominent cause of super-diffusive field line transport leading to a rapid exchange of particles and energy between resonant layers. Since poloidally diverted tokamaks with high plasma pressures are much more sensitive to resonant helical error fields and MHD instabilities, it is necessary to use external magnetic perturbation coils to control error field effects such as locked and resistive wall modes. These control coils induce a multiplicity of resonant magnetic island layers with their associated homoclinic tangles on many rational surfaces thus adding to the complexity of the magnetic topology and a need to better understand the combined effects of all the resonant perturbations on each rational surface.

We conclude by reminding the reader, in the words of M. Berry [3], "It must be emphasized that all this is in no sense pathological. It is the *generic situation* for solutions of Hamilton's equations."

REFERENCES

[a]Department of Mathematics, Cornell University, Ithaca New York.
[b]Harvard University, Cambridge Massachusetts.

[1] A. Lichtenberg and M. A. J. Lieberman, *Regular and Stochastic Motion*. Springer-Verlag, New York (1983).

[2] J. J. Palis and W. de Melo, *Geometric theory of dynamical systems: an introduction*. Springer-Verlag, New York (1982).

[3] M. V. Berry, in *Topics in nonlinear dynamics: a tribute to Sir Edward Bullard La Jolla Institute* American Institute of Physics, New York (1978) pp. 16-120.

[4] R. K. W. Roeder, T. E. Evans, and B. Rapoport, Bull. Am. Phys. Soc. **46**, 39 (2001).

[5] K. Elsässer, Plasma Physics and Controlled Fusion **28**, 1743 (1985).

[6] J. W. Bates and H. R. Lewis, Phys. Plasmas **4**, 2619 (1997).

[7] R. D. Hazeltine and J. D. Meiss, *Plasma Confinement*. Frontiers in Physics Vol. 89. Addison Wesley, New York (1992).

[8] B. V. Chirikov, Phys. Reports **52**, 263 (1979).

[9] J. M. Greene, J. Math. Phys. (NY or Cambridge, MA?) **20**, 1183 (1979).

[10] J. V. José and E. J. Saletan, *Classical Dynamics*. Cambridge University Press, Cambridge, Massachusetts (1998).

[11] J. Guckenheimer and P. Holmes, *Nonlinear Oscillations, Dynamical Systems, and Bifurcations of Vector Fields*. Springer-Verlag, New York (1983).

[12] P. Holmes, Physics Reports **193**, 137 (1990).

[13] V. K. Melnikov, Doklady akademii nauk SSSR **144**, 474 (1962).

[14] R. Balescu, M. Vlad, and F. Spineanu, Phys. Rev. E **58**, 951 (1998).

[15] T. E. Evans, in *Proceedings of the 18th European Physical Society Conference on Controlled Fusion and Plasma Physics*, Berlin, 1991, Vol. 15C, Part II (European Physical Society, Petit-Lancy, 1991) p. 65.

[16] A. Punjabi, A. Verma and A. Boozer, Phys. Rev. Lett. **69**, 3322 (1992).

[17] H. E. Nusse and J. A. Yorke, *Numerical Explorations*. Springer-Verlag, New York (1994).

Acknowledgments

This is a report of work supported by the U.S. Department of Energy under Contract No. DE-AC03-99ER54463 and by a NDSEG Fellowship, a National Undergraduate Fusion Fellowship. The authors would like to thank J.M. Greene for his careful reading of this paper.